Soft Matter

Accepted Manuscript

ROYAL SOCIETY OF CHEMISTRY

www.rsc.org/softmatter

Tuning the mesogenic properties of phenoxy-terminated smectic liquid crystals: the effect of fluoro substitution

Matthew Thompson,[a] Carolyn Carkner,[a] Nicholas J. Mosey,[a] Nadia Kapernaum[b] and Robert P. Lemieux*,[a]

[a]*Chemistry Department, Queen's University, Kingston, Ontario, Canada*

[b]*Institute of Physical Chemistry, Universität Stuttgart, Pfaffenwaldring 55, D-70569 Stuttgart, Germany*

Email: lemieux@chem.queensu.ca

Table of Content Entry

The mesogenic properties of phenoxy-terminated liquid crystals can be tuned with fluoro substituents on the phenoxy end-group.

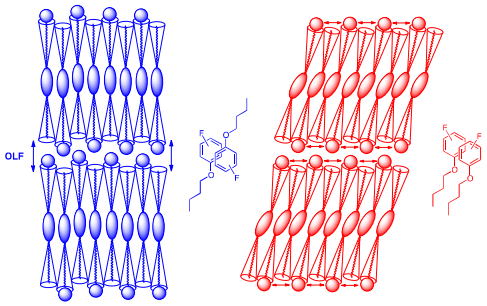

Abstract

The mesogenic properties of phenoxy-terminated 5-alkoxy-2-(4-alkoxyphenyl)pyrimidine liquid crystals can be tuned in a predictable fashion with fluoro substituents on the phenoxy end-group. We show that an *ortho*-fluoro substituent promotes the formation of a tilted smectic C (SmC) phase whereas a *para*-fluoro substituent promotes the formation of an orthogonal smectic A (SmA) phase. The balance between SmA and SmC phases may be understood in terms of the energetic preference of the phenoxy end-groups to self-assemble via arene-arene interactions in a parallel or antiparallel geometry, and how these non-covalent interactions may cause either a suppression or enhancement of out-of-layer fluctuations at the interface of smectic layers. Calculations of changes in the potential energy of association ΔE for non-covalent dimers of fluoro-substituted *n*-butyloxybenzene molecules in parallel and antiparallel geometries support this hypothesis. We also show how mesogenic properties can be further tuned by difluoro and perfluoro substitution, including difluoro substitution at the *ortho* positions, which uniquely promotes the formation of a SmC-nematic phase sequence.

Introduction

Rod-shaped organic compounds that self-organize in fluid lamellar structures are known as *smectic liquid crystals* and normally consist of molecules with a rigid aromatic core and flexible alkyl chains.[1] The most commonly observed smectic phases are the smectic A (SmA) and smectic C (SmC) phases, which have diffuse lamellar structures described by a density wave with a period d corresponding to the layer spacing.[2] In the uniaxial SmA phase, the director **n** corresponding to the average orientation of long molecular axes is coincident with the smectic layer normal **z**; in the biaxial SmC phase, **n** is tilted relative to **z** by an angle θ that varies with temperature. The study of structure-property relationships in smectic liquid crystals has been motivated in particular by Meyer's discovery of the ferroelectric properties of chiral SmC* liquid crystals,[3] and the application of these materials in surface-stabilized ferroelectric liquid crystal (SSFLC) electro-optical switches (Fig. 1), which are used commercially in reflective liquid-crystal-on-silicon microdisplays.[4-7]

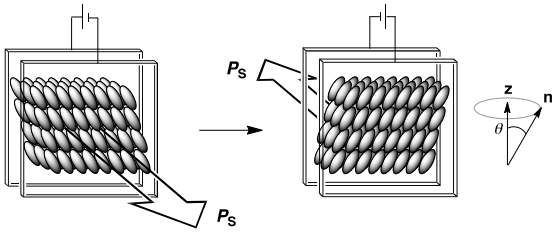

Fig. 1. Schematic representation of hard spherocylinders forming a chiral SmC* phase as a surface-stabilized ferroelectric liquid crystal (SSFLC) film between ITO glass slides with a rubbed alignment substrate, and the Goldstone mode switching described by the conical motion of the director **n** about the layer normal **z**, which is driven by the coupling of an applied electric field E to the spontaneous polarization P_S of the SSFLC.

Commercial FLC formulations normally consist of an achiral host mixture forming nematic (N) and SmA phases above the SmC phase, and a chiral dopant to induce a spontaneous polarization P_S in the SmC phase. The resulting N*-SmA*-SmC* phase sequence is required to achieve a uniform alignment of the FLC between glass slides with a low pretilt rubbed polyimide or nylon substrate upon cooling from the isotropic (I) liquid phase. Diverse libraries of achiral materials are required to optimize a wide range of physical parameters in FLC mixtures, including temperature range, Goldstone mode viscosity, optical tilt angle, resistivity and

birefringence.[6] Tuning the mesogenic properties of smectic liquid crystals has focused primarily on structural modifications of the rigid aromatic core based on the assumption that lamellar ordering is driven by the amphiphilicity of mesogens,[8, 9] and that variations in van der Waals interactions between aromatic cores should have a pronounced effect on mesogenic properties.[1, 10, 11] However, studies have shown that the introduction of functional end-groups on one alkyl chain can have significant effects on mesogenic properties, although the exploitation of this approach in tuning mesogenic properties has been narrower in scope.[12-14] For example, siloxane and carbosilane end-groups are well know to promote high lamellar order and stabilize the tilted SmC phase by nanosegregating from the hydrocarbon segments to form intercalated smectic bilayers; this nanosegregation results in a partial suppression of out-of-layer fluctuations, which reduces the entropic cost of molecular tilt by rod-like (calamitic) mesogens.

We have exploited the nanosegregation effect of siloxane and carbosilane end-groups in the design of 'de Vries-like' liquid crystals, which undergo a SmA-SmC phase transition with a layer contraction of <1% and have the potential to solve the intractable problem of chevron formation in SSFLC displays.[7, 15] The design features of these materials include a trisiloxane or tricarbosilane end-group together with a SmA-promoting element such as a chloro-terminated alkyl chain or a 5-phenylpyrimidine core.[16] By systematically varying the length of the carbosilane end-group, we recently showed that 'de Vries-like' properties depend strongly on the degree of nanosegregation and quality of lamellar ordering imposed by the end-group.[17] In the process of developing a diverse library of 'de Vries-like' mesogens, we have sought to expand the scope of nanosegregating elements in a new design that includes phenoxy end-groups,[18] which should segregate from alkyl chains at the smectic layer interface by virtue of their strong non-covalent interactions, and perhaps enable the tuning of mesogenic properties by appropriate aromatic substitution.[19] There are few reports of arene-terminated mesogens in the literature, which are mostly limited to homologous series of nematogens that exhibit pronounced odd-even effects in their N-I transition temperatures.[20-25]

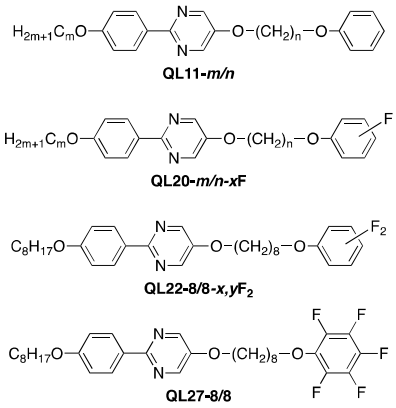

Our first study focused on a sterically equivalent series of phenoxy-terminated 5-alkoxy-2-(4-alkoxyphenyl)pyrimidine liquid crystals **QL11-*m/n***, where $m + n = 16$, which allowed us to investigate the interplay between core-core interactions and the effect of the phenoxy end-group on lamellar ordering.[18] A comparison of the mesogenic properties of **QL11-*m/n*** with those of the parent isomers lacking the end-group (**2PhP-*m/n***) showed that the phenoxy end-group causes a significant increase in melting point and reduces the mesogenic range of these materials. In most cases, the broad enantiotropic SmC phase formed by the parent isomers is suppressed by the addition of the phenoxy end-group. An analysis of the SmA phase formed by **QL11-10/6** using small angle and 2D X-ray scattering was consistent with an intercalated bilayer structure in which the phenoxy end-groups are nanosegregated. Molecular modeling also revealed that differences in mesogenic properties between the representative isomers **QL11-8/8**, **QL11-10/6** and **QL11-12/4** (Fig. 2) may be explained by differences in energies of core-core interactions imposed by the nanosegregation of the phenoxy end-groups in the proposed intercalated bilayer structure.

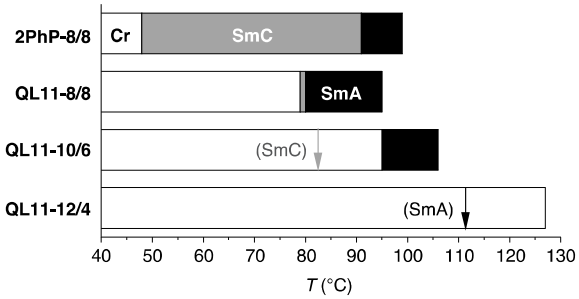

Fig. 2. Mesophases formed by the parent compound 5-octyloxy-2-(4-octyloxyphenyl)pyrimidine (**2PhP-8/8**) and the phenoxy-terminated derivative **QL11-8/8**, and by the sterically equivalent isomers **QL11-10/6** and **QL11-12/4**. The arrows represent monotropic phase transitions (data taken from ref. 18).

In this paper, we report a detailed study of the effect of fluoro substitution on the mesogenic properties of the phenoxy-terminated liquid crystals **QL11-*m/n*** and show how it may provide a predictable means of tuning the properties of FLC mixtures in a synthetically convenient manner. Aromatic fluoro substitution is a powerful approach to tuning the properties of nematic and ferroelectric liquid crystals for display applications without compromising liquid crystallinity because of the small size, high polarity and high chemical stability of the fluoro group.[11, 26] Lateral fluoro substituents on aromatic cores have been widely used in the development of nematic liquid crystals with high negative dielectric anisotropy for vertically aligned nematic (VAN) display applications, and achiral SmC liquid crystals with low viscosity and high resistivity. Notably, the development of difluoroterphenyl mesogens by Gray *et al.* proved to be a major innovation in LCD technology that also demonstrated how mesogenic properties can be drastically modified by changing the positions of fluoro substituents on the terphenyl core.[27] We show herein how changing the position of a single fluoro substituent on the phenoxy end-group of **QL11-*m/n*** can affect its mesogenic properties, and provide an explanation for the substituent effects in terms of arene-arene interactions at the smectic layer interfaces and their possible influence in promoting or suppressing out-of-layer fluctuations. We also show how mesogenic properties can be further tuned by difluoro and perfluoro substitution.

Results and discussion

Synthesis and characterization. The compounds **QL20-*m/n*-*x*F, QL22-8/8-*x,y*F$_2$** and **QL27-8/8** were prepared by sequential alkylations of 2-(4-hydroxyphenyl)pyrimidin-5-ol with the appropriate fluorophenoxy-terminated 1-bromoalkane and 1-bromoalkane via nucleophilic substitution reactions (see ESI for full synthetic details). The new compounds were recrystallized from acetonitrile and hexane, and their mesogenic properties were characterized by polarized optical microscopy (POM) and differential scanning calorimetry. Phase transition temperatures and enthalpies of transition are listed in Table 1.

Table 1. Transition temperatures (°C) and enthalpies of transitions (kJ mol^{-1}, in parentheses) for compounds **QL20-*m*/*n*-*x*F**, **QL22-8/8-*x*,*y*F$_2$** and **QL27-8/8** measured by DSC.

Compound	Cr		SmC		SmA	N		I
QL20-8/8-2F	•	66 (56)	•	80[a]	•		83 (9.3)	•
QL20-8/8-3F	•	81 (42)	(•	72)[a,c]	•		96 (12)	•
QL20-8/8-4F	•	82 (46)			•		102 (10)	•
QL20-10/6-2F	•	72 (37)	•	85[a]	•		88 (9.2)	•
QL20-10/6-3F	•	87 (50)	(•	75)[a,c]	•		106 (12)	•
QL20-10/6-4F	•	93 (41)			•		114 (12)	•
QL20-12/4-2F	•	91	(•	85)[a,c]	•		93 (49)[b]	•
QL20-12/4-3F	•	120 (52)			(•		116 (8.5))[c]	•
QL20-12/4-4F	•	120 (51)			•		133 (13)	•
QL22-8/8-2,3F$_2$	•	81 (63)	(•	78)[a,c]	•		88 (11)	•
QL22-8/8-2,4F$_2$	•	62 (56)	(•	61)[a,c]	•		92 (10)	•
QL22-8/8-2,5F$_2$	•	75 (42)	•	76[a]	•		87 (10)	•
QL22-8/8-2,6F$_2$	•	36 (22)	•	68 (2.5)		•	75 (1.7)	•
QL22-8/8-3,4F$_2$	•	78 (51)			•		98 (8.9)	•
QL22-8/8-3,5F$_2$	•	88 (52)			•		95 (12)	•
QL27-8/8	•	36 (19)	•	65[a]	•		92 (9.3)	•

[a] Transition temperature measured by polarized microscopy. [b] Total enthalpy for both transitions due to partial resolution of the peaks. [c] Monotropic mesophase.

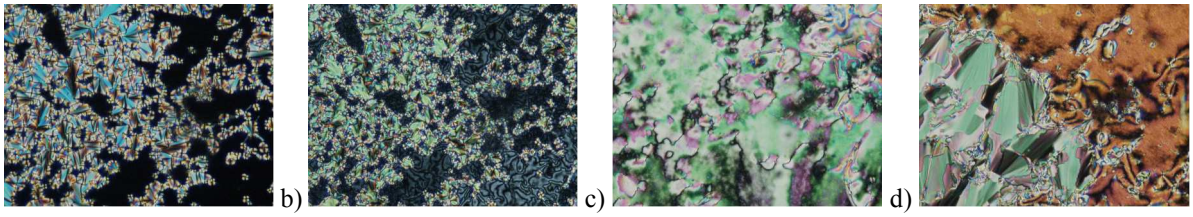

Fig. 3. Polarized photomicrographs of (a) **QL20-8/8-2F** in the SmA phase at 82 °C, (b) **QL20-8/8-2F** in the SmC phase at 69 °C, (c) **QL22-8/8-2,6F$_2$** in the N phase at 73 °C, and (d) **QL22-8/8-2,6F$_2$** in the SmC phase at 67 °C, all acquired on cooling from the isotropic liquid phase.

The SmA phase was identified by the formation of characteristic fan textures and dark homeotropic domains on cooling from the isotropic liquid phase, as shown in Fig. 3a; for the applicable compounds, the SmC phase was identified on further cooling from the SmA phase by the appearance of Schlieren textures in the homeotropic domains and the conversion of fan textures to characteristic broken fans textures, as shown in Fig. 3b.[28] The nematic phase formed by **QL22-8/8-2,6F$_2$** was identified by the formation of a marbled texture with high birefringence, which turned into Schlieren and fan textures upon transition to the SmC phase, as shown in Figs.

3c and 3d. The absence of broken fans is characteristic of a SmC phase formed via a first-order SmC-N transition.[28]

In the monofluoro series **QL20-*m/n-x*F**, we chose to examine the same three representative isomers featured in Fig. 2, which reflect the interplay between core-core interactions and the nanosegregation imposed by the phenoxy end-groups. Modeling of intermolecular correlations in the SmA phase formed by the parent isomers **QL11-*m/n*** suggest that the phenylpyrimidine cores are approximately in register in the intercalated bilayer structure formed by **QL11-10/6**, and partially offset to bring the pyrimidine rings in register in the case of **QL11-8/8**, and the phenyl rings in register in the case of **QL11-12/4**.[18] As shown in Fig. 4, the trend in mesogenic properties observed with the three **QL11-*m/n*** isomers, i.e., the increase in melting point and reduction in mesogenic character with decreasing length *n* of the phenoxy-terminated alkoxy chain, is also observed with compounds **QL20-*m/n-x*F**, which suggests that a similar intercalated bilayer structure is formed in their smectic phases.

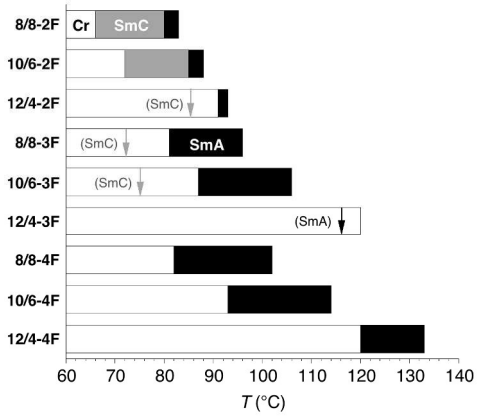

Fig. 4. Mesophases formed by the phenoxy-terminated derivatives **QL20-*m/n-x*F**. The arrows represent monotropic phase transitions.

Far more interesting is the effect of changing the position of the fluoro substituent from the *ortho* to the *para* position on the phenoxy end-group. Notwithstanding that all nine monofluoro derivatives form a SmA phase, including **QL20-12/4-3F**, which forms a SmA phase on cooling only (monotropic), the effect of the *ortho*-fluoro substituent is distinct and twofold: (i) it causes

an appreciable decrease in melting point and (ii) it promotes the formation of a SmC phase, even with the 12/4 isomer as a monotropic phase; a similar melting point depression was recently observed upon *ortho*-fluorination of the phenyl-terminated nematogen 4-cyano-4'-(11-phenylundecyloxy)biphenyl.[25] On the other hand, the *para*-fluoro substituent stabilizes the SmA phase and completely suppresses the formation of the SmC phase, even on cooling. The effect of the *meta*-fluoro substituent appears to be somewhere in between those of *ortho* and *para* to the extent that it is negligible. Indeed, the mesogenic properties of the three *meta*-fluoro isomers are nearly identical to those of the parent isomers **QL11-*m/n***.

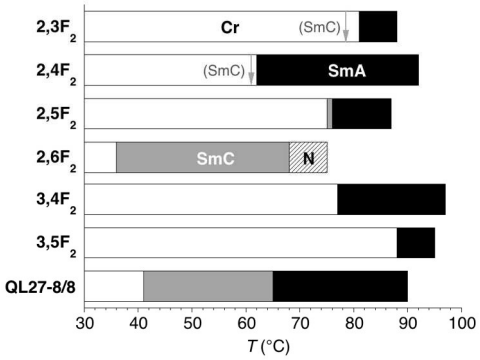

Fig. 5. Mesophases formed by the phenoxy-terminated derivatives **QL22-8/8-*x,y*F$_2$** and **QL27-8/8**. The arrows represent monotropic phase transitions.

In the difluoro substituted series **QL22-8/8-*x,y*F$_2$**, the opposing substituent effects appear to balance one another. As shown in Fig. 5, the 2,3-, 2,4- and 2,5-regioisomers form SmA and SmC phases, although the SmC phase is monotropic in two cases. Perhaps coincidentally, the mesogenic properties of the 2,5-regioisomer, in which the two fluoro substituents are in direct opposition, are almost identical to those of the unsubstituted analogue **QL11-8/8**. In the absence of an *ortho*-fluoro substituent, *viz*., the 3,4- and 3,5-regioisomers, only a SmA phase is formed. On the other hand, having fluoro substituents at both *ortho* positions results in the formation of a nematic phase and a very broad SmC phase; this is a less common phase sequence that may have interesting implications in terms of chevron-free SSFLC devices (vide infra). In the case of the perfluorinated derivative **QL27-8/8**, we observed broad SmA and SmC phases and a significant lowering of the melting point, which is consistent with a report by Itahara on the effect of a

perfluorophenoxy end-group on the mesogenic properties of a homologous series of 4-alkoxy-4'-cyanobiphenyl nematogens.[23] On cooling from the isotropic liquid phase, the SmC phase of **QL27-8/8** persists at temperatures as low as 2 °C due to substantial supercooling.

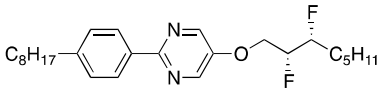

MDW797

Optical tilt angle measurements. Optical tilt angles (θ_{opt}) in the SmC phase were first measured by POM in the absence of an electric field as half the angle of rotation between dark states in domains of opposite tilt orientation with the samples aligned in ITO glass cells with a cell gap of 4 μm and a low pretilt (< 1°) rubbed polyimide alignment substrate. Measurements of θ_{opt} for **QL20-8/8-2F** and **QL20-10/6-2F** gave unusually low values of 6-8° at a reduced temperature of 10 K below the SmA-SmC phase transition point ($T–T_{AC}$ = –10 K), which were consistent with those previously reported for **QL11-10/6** under similar conditions.[18] To assess the validity of these measurements, the samples were doped with the chiral additive **MDW797** (2-5 mol%) and tilt angles were measured electro-optically by switching the SmC* phase between opposite tilt orientations as SSFLC films aligned in the same glass cells. Unlike conventional FLC materials, the $\theta_{opt}(T)$ profiles of **QL20-8/8-2F**, **QL20-10/6-2F**, **QL20-10/6-3F** and **QL22-8/8-2,6F$_2$**, as well as the unsubstituted analogue **QL11-8/8**, showed a pronounced dependence on the applied field E, and brought into question the measurements reported for **QL11-10/6**.[18]

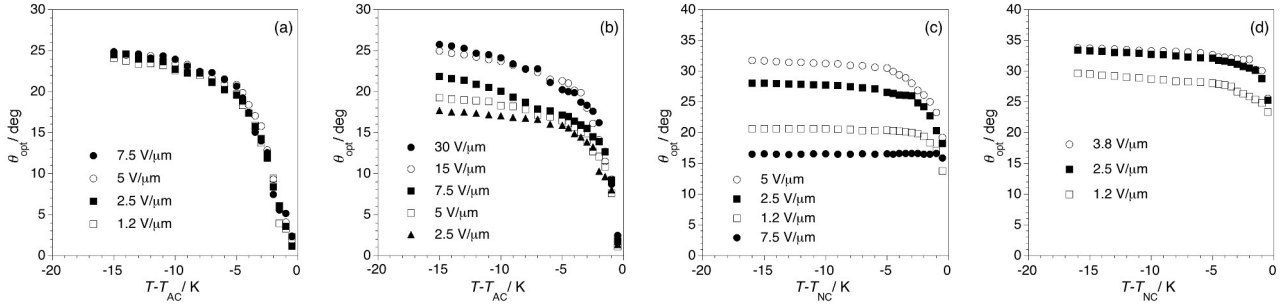

Fig. 6. Optical tilt angle *vs.* reduced temperature measured electro-optically by POM at various electric fields in the SmC* phase for three mesogens doped with the chiral additive **MDW797** (x mol%): (a) **2PhP-8/8** (2 mol%), (b) **QL20-10/6-2F** (5 mol%), (c) **QL22-8/8-2,6F$_2$** (2 mol%) and (d) **QL22-8/8-2,6F$_2$** (5 mol%).

For example, the optical tilt of **QL20-10/6-2F** gradually increases with E and reaches a saturation point at 15 V μm^{-1}, whereas the $\theta_{opt}(T)$ profile of the conventional mesogen **2PhP-8/8** shows no such dependence, as shown in Figs. 6a and 6b. The increase in θ_{opt} with E persists well below the SmA-SmC transition point T_{AC} and is therefore inconsistent with an electroclinic effect, which is only observed in the near vicinity of T_{AC} and is usually very small in the SmC* phase—on the order of 1-2°.[29-31] The saturation voltage decreases with increasing dopant concentration—from 2 to 5 mol%—and a saturation of $\theta_{opt}(E)$ is observed in all cases except for **QL22-8/8-2,6-F$_2$** with 2 mol% of **MDW797**, as shown in Fig. 6c. The optical tilt of this SmC* mixture increases with E up to 5 V μm^{-1}, and then decreases by ca. 50% with a further increase in E to 7.5 V μm^{-1}. However, this effect vanishes with a higher dopant concentration of 5 mol%, and a saturation of $\theta_{opt}(E)$ is observed at 2.5 V μm^{-1}.

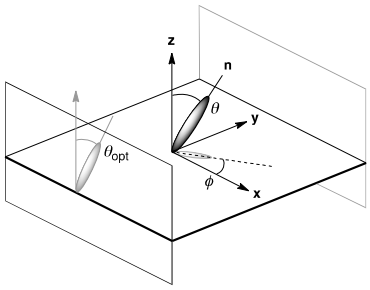

Fig. 7. Local symmetry of the SmC* phase in a surface-stabilized configuration between two glass slides. The mesogen is represented by a hard spherocylinder oriented along the director **n**; its projection in the tilt plane **xz** is shown in grey (adapted from ref. 6a).

These results suggest that the phenoxy end-groups cause an appreciable pretilt ϕ of the director **n** about the tilt cone in the SmC* phase. As shown in Fig. 7, this pretilt should give an optical tilt angle θ_{opt} that appears by POM to be less than the actual tilt angle θ in the absence of an applied field. With the electro-optical measurements of $\theta_{opt}(T)$, the ferroelectric torque Γ produced by the coupling of E to the spontaneous polarization P_S induced by **MDW797**, which drives the Goldstone mode switching described in Fig. 1, should also work against the pretilt elasticity to bring the director **n** in the tilt plane **xz** at the saturation voltage.[6] In this context, the anomalous $\theta_{opt}(E)$ behavior of the 2,6-difluorophenoxy derivative with 2 mol% of **MDW797** may be explained by considering the opposing effects of dielectric and ferroelectric torques. In

the SmC* phase, the **z** component of the dielectric torque Γ^{ε} working on ϕ is proportional to E^2 and the dielectric anisotropy and/or dielectric biaxiality of the liquid crystal, whereas the ferroelectric torque Γ is proportional to E and P_S.[6] Hence, the $\theta_{opt}(E)$ behavior described in Fig. 6c may be explained by competing Γ and Γ^{ε}, with the latter dominating at higher E and driving the director **n** away from the tilt plane. A higher concentration of **MDW797** (5 mol%) would restore the dominance of the ferroelectric torque by virtue of a higher P_S and thus allow tilt saturation to be achieved. The fact that this behavior is only observed with **QL22-8/8-2,6F$_2$** is consistent with molecular models suggesting that the two *ortho*-fluoro substituents should increase the positive dielectric anisotropy of the liquid crystal (see Fig. S1 in ESI).

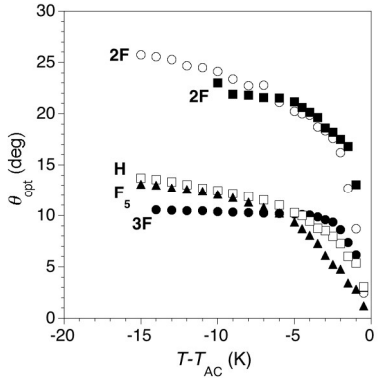

Fig. 8. Optical tilt angle *vs.* reduced temperature measured electro-optically by POM at 15 V μm^{-1} in the SmC* phase for five mesogens doped with the chiral additive **MDW797** (5 mol%): **QL11-8/8** (□), **QL20-8/8-2F** (■), **QL20-10/6-2F** (○) **QL20-10/6-3F** (●) and **QL27-8/8** (▲). The data were acquired on cooling from the isotropic liquid phase.

As shown in Fig. 8, the SmC promoting effect of the *ortho*-fluoro substituent is seen in the larger optical tilt angles of 23° and 24° at $T–T_{AC} = –10$ K for **QL20-8/8-2F** and **QL20-10/6-2F**, respectively; these are more than twice the optical tilt angles measured at the same reduced temperature for the unsubstituted mesogen **QL11-8/8**, the *meta*-fluoro derivative **QL20-10/6-3F** and the perfluoro derivative **QL27-8/8**, in which the opposing effects of *ortho*- and *para*-fluoro substituents appear to cancel out. Further evidence of this SmC-promoting effect is provided by the step function-like $\theta_{opt}(T)$ profile of **QL22-8/8-2,6F$_2$** (Fig. 6d), which is typical of liquid crystals with a first-order SmC-N phase transition, showing a tilt angle of 33° at $T–T_{AC} = –10$ K.

Small angle X-ray scattering. The three fluorinated mesogens forming enantiotropic SmA and SmC phases over appreciable temperature ranges were analyzed by small angle X-ray scattering (SAXS) as a function of temperature to determine the extent of smectic layer contraction on transition from the orthogonal SmA to the tilted SmC phase. The smectic layer spacing d was derived from the first order scattering peak at small angle on heating from the crystalline phase, except for the non-fluorinated mesogen **QL11-8/8**, which was analyzed on cooling from the isotropic phase due to the narrow temperature range of the SmC phase on heating. As shown in Fig. 9, the profiles of relative layer spacing d/d_{AC} *vs.* reduced temperature show a substantial degree of layer contraction upon transition to the SmC phase at T_{AC}, which is typically observed with conventional smectic liquid crystals. The difference in layer contraction between the two *ortho*-fluorinated mesogens and the non-fluorinated mesogen **QL11-8/8** can be accounted for by the difference in tilt angle θ_{opt}. Indeed, the reduction factor R values calculated at $T–T_{AC} = –10$ K for these three compounds range from 0.80 to 0.87, which are the same within experimental error (assuming errors of ± 0.1 Å for SAXS and ± 1° for θ_{opt} measurements), and suggest the absence of 'de Vries-like' properties.[32] The $d/d_{AC}(T)$ profile of the perfluorinated mesogen **QL27-8/8** is very similar to that of **QL11-8/8**, and gives an R value approaching 1 at $T–T_{AC} = –10$ K.

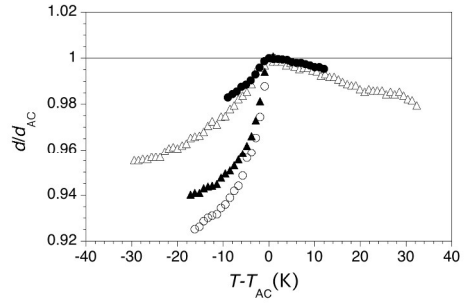

Fig. 9. Relative smectic layer spacing *vs.* reduced temperature for **QL11-8/8** (●), **QL20-8/8-2F** (▲), **QL20-10/6-2F** (○) and **QL27-8/8** (△). The data were acquired on heating from the crystalline phase except for **QL11-8/8**.

Modeling of end-group interactions. To understand the effect of fluoro substitution on the mesogenic properties reported herein, we modeled the interactions of phenoxy end-groups at the interface of smectic layers by calculating changes in the potential energy of association ΔE for

non-covalent dimers of fluoro-substituted *n*-butyloxybenzene molecules in parallel and antiparallel geometries. At a first-order of approximation, these two geometries model the non-covalent interactions of phenoxy end-groups within a smectic layer and between layers through out-of-layer fluctuations (OLF), respectively, as shown in Fig. 10. The assumption underlying this modeling exercise is that the suppression of out-of-layer fluctuations due to attractive non-covalent interactions between phenoxy end-groups in a parallel geometry should favor the SmC phase by reducing the entropic cost of molecular tilt. On the other hand, attractive non-covalent interactions between phenoxy end-groups in an antiparallel geometry would require out-of-layer fluctuations, which are less hindered in the orthogonal SmA phase, as illustrated in Fig. 10.

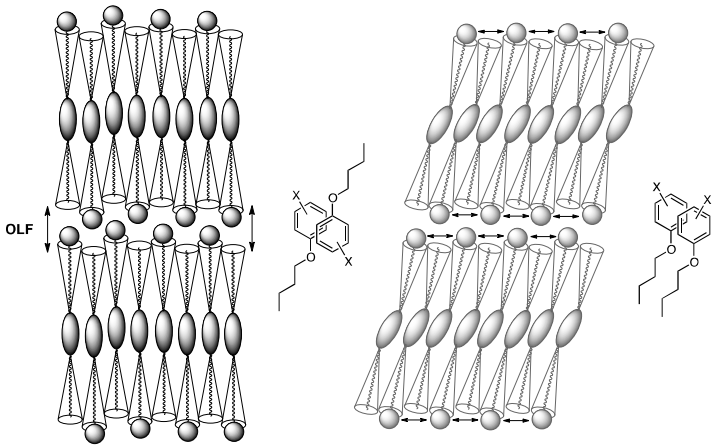

Fig. 10. Models of phenoxy end-group interactions in antiparallel and parallel geometries in relation to structures of the SmA (left) and SmC phases (right).

Calculations were performed with starting dimer geometries in which the two molecules are oriented either parallel or antiparallel, and the aromatic rings are perfectly superposed; with the ortho- and *meta*-fluoro derivatives, separate starting geometries with the fluoro substituents oriented in the same (*syn*) or opposite (*anti*) directions were used. The potential energies of the systems were obtained at the MP2/6-311++G**//MP2/6-31+G** level of theory using the Gaussian 09 software package,[33] and corrected for basis set superposition error (BSSE) using the counterpoise method.[34] In each case, ΔE was calculated as the difference between the BSSE-corrected energy of the associated dimer and twice the energy of one molecule obtained at the MP2/6-311++G**//MP2/6-31+G** level. In all cases, the parallel or antiparallel orientations

imposed at the start of the minimizations were closely maintained in the final structures, as shown by four representative examples in Fig. 11. The resulting ΔE values are listed in Table 2.

Table 2. Potential energies of association ΔE for unsubstituted and fluoro-substituted *n*-butyloxybenzene dimers in parallel and antiparallel geometries.[a]

	ΔE (kcal mol^{-1})[b]			
X	*Parallel-Syn*	*Parallel-Anti*	*Antiparallel-Syn*	*Antiparallel-Anti*
H	–6.8		–6.5	
2F	–6.2	–7.5	–4.3	–6.5
3F	–6.2	–6.8	–6.3	–6.4
4F	–8.1		–9.2	

[a] Based on BSSE-corrected energies obtained at the MP2/6-311++G**//MP2/6-31+G** level of theory.
[b] Calculated as the difference between the BSSE-corrected energy of the associated dimer and twice the energy of one molecule obtained at the MP2/6-311++G**//MP2/6-31+G** level.

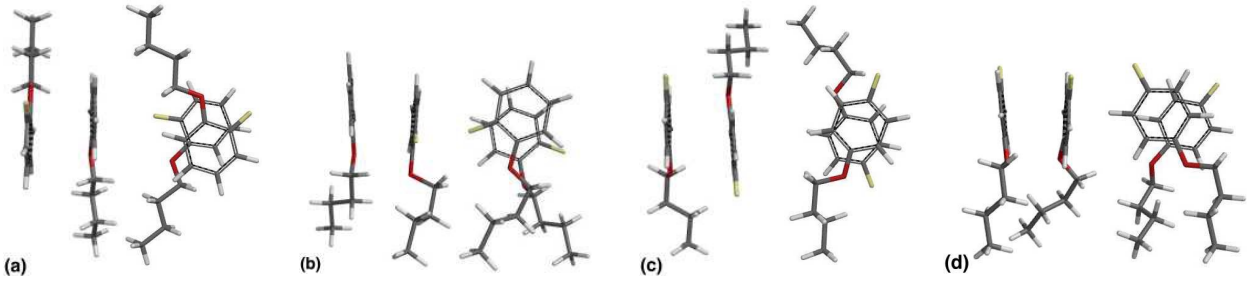

Fig. 11. Dimer geometries minimized at the MP2/6-31+G** level as side and front views: (a) 1-(*n*-butyloxy)-2-fluorobenzene (*antiparallel-anti*), (b) 1-(*n*-butyloxy)-2-fluorobenzene (*parallel-anti*), (c) 1-(*n*-butyloxy)-4-fluorobenzene (*antiparallel*), and (d) 1-(*n*-butyloxy)-4-fluorobenzene (*parallel*).

Notwithstanding the usual caveat about drawing correlations between calculated energies of non-covalent interactions in the gas phase and bulk properties in the condensed phase, and considering that all calculations were performed at the same level of theory on structurally similar systems, the trend in association energy difference $\Delta\Delta E$ between the most stable parallel and antiparallel geometries of fluoro-substituted *n*-butyloxybenzene dimers is consistent with the observed substituent effects.[35] Hence, the difference in association energy $\Delta\Delta E$ between the parallel and antiparallel *anti* geometries of the *ortho*-fluoro dimer is 1.0 kcal mol^{-1} in favor of the parallel geometry, whereas the corresponding energy difference $\Delta\Delta E$ for the *para*-fluoro dimer is

1.1 kcal mol^{-1} in favor of the antiparallel geometry.[36] The $\Delta\Delta E$ for the *meta*-fluoro dimer and unsubstituted dimer are smaller (0.3-0.4 kcal mol^{-1}), although opposite geometries are favored. This may be consistent with the fact that a *meta*-fluoro substituent has a negligible effect on the smectogenic properties of phenoxy-terminated mesogens, and that the more subtle energetic preference for phenoxy end-group interactions in either a parallel or antiparallel geometry may not be strong enough to affect the inherent balance between SmA and SmC phases formed by these materials.

Conclusions.

Using the well-known 2-phenylpyrimidine scaffold, we have shown that the mesogenic properties of phenoxy-terminated liquid crystals can be tuned in a predictable fashion by the use of fluoro substituents. This approach is particularly attractive from a synthetic point of view since libraries of derivatized phenoxy-terminated alkyl chain precursors are easy to prepare and can be introduced in a variety of scaffolds, avoiding the need to derivatize aromatic cores. We showed that a single *ortho*-fluoro substituent promotes the formation of a tilted SmC phase whereas a single *para*-fluoro substituent promotes the formation of an orthogonal SmA phase. The balance between SmA and SmC phases may be understood in terms of the energetic preference for the phenoxy end-groups to self-assemble via arene-arene interactions in a parallel or antiparallel geometry, and how these non-covalent interactions cause either a suppression or enhancement of out-of-layer fluctuations at the interface of smectic layers that tips the balance towards a SmC or SmA phase, respectively. Calculations of changes in the potential energy of association ΔE for non-covalent dimers of fluoro-substituted *n*-butyloxybenzene molecules in parallel and antiparallel geometries are consistent with this hypothesis. Electro-optical measurements also showed that phenoxy end-groups cause an appreciable pretilt of the director **n** about the tilt cone in the SmC phase, which is normally absent in commercial FLC formulations.

Finally, we showed that a 2,6-difluorophenoxy end-group uniquely promotes the formation of a nematic and a SmC phase, which is a less commonly observed phase sequence, although preliminary experiments on different mesogenic scaffolds suggest that this substituent effect is general. This may be related to the unique conformation of the 2,6-difluorophenoxy end-group in which the alkoxy group is orthogonal to the plane of the aromatic ring (see Fig. S1 in ESI). The first-order N-SmC transition normally gives rise to an optical tilt angle that is invariant of temperature, and can therefore lead to the formation of a chevron-free SSFLC film that might be useful in device applications provided it can be uniformly aligned in ITO glass cells with rubbed alignment substrates. However, the positive dielectric anisotropy of **QL22-8/8-2,6F$_2$** is not ideal to achieve a uniform alignment on cooling from the N to the SmC phase using an applied electric field due to the Freedericksz transition in the N phase that drives the director away from the planar orientation imposed by the alignment substrate. To solve this problem, we are developing new 2,6-difluorophenoxy-terminated mesogens with a negative dielectric anisotropy and will report on these new materials in due course.

Acknowledgments

We thank the Natural Sciences and Engineering Research Council of Canada (Discovery and CREATE grants), the Deutsche Forchungsgemeinschaft (NSF/DFG *Materials World Network* program DFG Gi 243/6), Westgrid and Compute Canada for support of this work. We also thank Dr. Michael Wand for a generous gift of **MDW797**, and Profs. Per Rudquist and Piotr Kaszynski for useful discussions.

References

1. J. W. Goodby, in *Handbook of Liquid Crystals*, eds. J. W. Goodby, P. J. Collings, T. Kato, C. Tschierske, H. F. Gleeson and P. Raynes, Wiley-VCH, Weinheim, 2014, vol. 4, pp. 3-41.
2. W. L. McMillan, *Phys. Rev. A*, 1971, **4**, 1238-1246.

3. R. B. Meyer, L. Liebert, L. Strzelecki and P. Keller, *J. Phys. (Paris) Lett.*, 1975, **36**, L69-71.

4. N. A. Clark and S. T. Lagerwall, *Appl. Phys. Lett.*, 1980, **36**, 899-901.

5. J. W. Goodby, R. Blinc, N. A. Clark, S. T. Lagerwall, M. A. Osipov, S. A. Pikin, T. Sakurai, K. Yoshino and B. Zeks, eds., *Ferroelectric Liquid Crystals: Principles, Properties and Applications*, Gordon & Breach, Philadelphia, 1991.

6. (a) S. T. Lagerwall, *Ferroelectric and Antiferroelectric Liquid Crystals*, Wiley-VCH, Weinheim, 1999; (b) S. T. Lagerwall, in *Handbook of Liquid Crystals*, eds., J. W. Goodby, P. J. Collings, T. Kato, C. Tschierske, H. F. Gleeson and P. Raynes, Wiley-VCH, Weinheim, 2014, vol. 8, pp. 213-236.

7. J. P. F. Lagerwall and F. Giesselmann, *ChemPhysChem.*, 2006, **7**, 20-45.

8. B. I. Ostrovskii, in *Structure and Bonding*, ed. D. M. P. Mingos, Springer-Verlag, Berlin, 1999, vol. 94, pp. 199-240.

9. C. Tschierske, in *Handbook of Liquid Crystals*, eds. J. W. Goodby, P. J. Collings, T. Kato, C. Tschierske, H. F. Gleeson and P. Raynes, Wiley-VCH, Weinheim, 2014, vol. 5, pp. 1-43.

10. J. W. Goodby, I. M. Saez, S. J. Cowling, J. S. Gasowska, R. A. MacDonald, S. Sia, P. Watson, K. J. Toyne, M. Hird, R. A. Lewis, S.-E. Lee and V. Vaschenko, *Liq. Cryst.*, 2009, **36**, 567-605.

11. (a) M. Hird, *Liq. Cryst.*, 2011, **38**, 1467-1493; (b) M. Hird, in *Handbook of Liquid Crystals*, eds., J. W. Goodby, P. J. Collings, T. Kato, C. Tschierske, H. F. Gleeson and P. Raynes, Wiley-VCH, Weinheim, 2014 Vol. 8, pp. 237-261.

12. J. W. Goodby, I. M. Saez, S. J. Cowling, V. Görtz, M. Draper, A. W. Hall, S. Sia, G. Cosquer, S.-E. Lee and E. P. Raynes, *Angew. Chem. Int. Ed.*, 2008, **47**, 2754-2787.

13. C. Tschierske, in *Handbook of Liquid Crystals*, eds. J. W. Goodby, P. J. Collings, T. Kato, C. Tschierske, H. F. Gleeson and P. Raynes, Wiley-VCH, Weinheim, 2014, vol. 5, pp. 45-88.

14. (a) C. Tschierske, *Isr. J. Chem.*, 2012, **52**, 935-959; (b) C. Tschierske, *J. Mater. Chem.*, 1998, **8**, 1485-1508.

15. Conventional FLC materials undergo a layer contraction of 7-10% on cooling from the SmA to the SmC phase; in a SSFLC film, this layer contraction causes a buckling of smectic layers into chevrons of opposite fold directions, which produces zigzag line defects that severely degrade the optical quality of the SSFLC film. Zigzag line defects can be avoided by controlling the chevron fold direction with appropriate surface treatment and alignment conditions, but the chevron geometry in SSFLC displays invariably results in lower brightness, contrast and viewing angle relative to a chevron-free bookshelf geometry. T. P. Rieker, N. A. Clark, G. S. Smith, D. S. Parmar, E. B. Sirota and C. R. Safinya, *Phys. Rev. Lett.*, 1987, **59**, 2658-2661.

16. (a) L. Li, C. D. Jones, J. Magolan and R. P. Lemieux, *J. Mater. Chem.*, 2007, **17**, 2313-2318; (b) J. C. Roberts, N. Kapernaum, Q. Song, D. Nonnenmacher, K. Ayub, F. Giesselmann, F. and R. P. Lemieux, *J. Am. Chem. Soc.,* 2010, **132**, 364-370; (c) Q. Song, D. Nonnenmacher, F. Giesselmann and R. P. Lemieux, *J. Mater. Chem. C,* 2013, **1**, 343-350; (d) C. P. J. Schubert, A. Bogner, J. H. Porada, K. Ayub, T. Andrea, F. Giesselmann and R. P. Lemieux, *J. Mater. Chem. C,* 2014, **2**, 4581-4589.

17. K. M. Mulligan, A. Bogner, Q. Song, C. P. J. Schubert, F. Giesselmann and R. P. Lemieux, *J. Mater. Chem. C*, 2014, **2**, 8270-8276.

18. M. Thompson, C. Carkner, A. Bailey, N. J. Mosey, N. Kapernaum and R. P. Lemieux, *Liq. Cryst.*, 2014, **41**, 1246-1260.

19. (a) L. M. Salonen, M. Ellermann and F. Diederich, *Angew. Chem. Int. Ed.*, 2011, **50**, 4808-4842; (b) R. K. Raju, J. W. G. Bloom, Y. An and S. E. Wheeler, *ChemPhysChem,* 2011, **12**, 3116-3130; (c) E. A. Meyer, R. K. Castellano and F. Diederich, *Angew. Chem. Int. Ed.,* 2003, **42**, 1210-1250; (d) C. A. Hunter, K. R. Lawson, J. Perkin and C. J. Urch, *J. Chem. Soc., Perkin Trans. 2*, 2001, **2**, 651-669.

20. (a) G. W. Gray and K. J. Harrison, *Mol. Cryst. Liq. Cryst.*, 1971, **13**, 37-60; (b) G. W. Gray, *J. Phys. (Paris),* 1975, **36**, 337-483; (c) D. Coates and G. W. Gray, *J. Phys. (Paris),* 1975, **36**, 365-374.

21. R. D. Ennulat and A. J. Brown, *Mol. Cryst. Liq. Cryst.*, 1971, **12**, 367-378.

22. W.-L. Tsai, H.-C. Lee, M.-Y. Hong, L.-N. Chen, M.-Y. Hu and F.-M. Hsu, *Liq. Cryst.*, 2004, **31**, 301-302.

23. T. Itahara, *Liq. Cryst.*, 2005, **32**, 115-118.

24. T. Itahara, A. Nishino, S. Furukawa and K. Kubota, *Liq. Cryst.*, 2013, **40**, 1167-1173.

25. R. J. Mandle, E. J. Davis, C.-C. A. Voll, D. J. Lewis, S. J. Cowling and J. W. Goodby, *J. Mater. Chem. C*, 2015, **3**, 2380-2388.

26. M. Hird, *Chem. Soc. Rev.*, 2007, **36**, 2070-2095.

27. G. W. Gray, M. Hird, D. Lacey and K. J. Toyne, *J. Chem. Soc., Perkin Trans. 2*, 1989, 2041-2053.

28. I. Dierking, *Textures of Liquid Crystals*, Wiley-VCH, Weinheim, 2003.

29. For a review, see: C. Bahr, in *Chirality in Liquid Crystals*, eds. H.-S. Kitzerow and C. Bahr, Springer-Verlag, New York, 2001, p. 223.

30. S. Garoff and R. B. Meyer, *Phys. Rev. Lett.*, 1977, **38**, 848-851.

31. F. Giesselmann and P. Zugenmaier, *Phys. Rev. E*, 1995, **52**, 1762-1772.

32. The degree of 'de Vries-like' behavior in a smectic liquid crystal may be quantified on a scale of 0 (perfect 'de Vries') to 1 (conventional SmA-SmC transition) at a given temperature T below T_{AC} by the reduction factor R according to the equation:

$$R = \delta(T)/\theta_{opt}(T) = \cos^{-1}[d_C(T)/d_{AC}]/\theta_{opt}(T)$$

where δ□ □) is the tilt angle required to give the observed layer contraction $d_C(T)/d_{AC}$ assuming a model of hard spherocylinders in which the layer contraction scales with the cosine of the tilt angle, and θ_{opt} is the optical tilt angle measured by polarized optical microscopy. Y. Takanishi, Y. Ouchi, H. Takezoe, A. Fukuda, A. Mochizuki and M. Nakatsuka, *Jpn. J. Appl. Phys.*, 1990, **2**, L984-L986.

33. Gaussian 09, Revision C.01, M. J. Frisch, G. W. Trucks, H. B. Schlegel, G. E. Scuseria, M. A. Robb, J. R. Cheeseman, G. Scalmani, V. Barone, B. Mennucci, G. A. Petersson, H. Nakatsuji, M. Caricato, X. Li, H. P. Hratchian, A. F. Izmaylov, J. Bloino, G. Zheng, J. L. Sonnenberg, M. Hada, M. Ehara, K. Toyota, R. Fukuda, J. Hasegawa, M. Ishida, T. Nakajima, Y. Honda, O. Kitao, H. Nakai, T. Vreven, J. A. Montgomery, Jr., J. E. Peralta, F. Ogliaro, M. Bearpark, J. J. Heyd, E. Brothers, K. N. Kudin, V. N. Staroverov, T. Keith, R. Kobayashi, J. Normand, K. Raghavachari, A. Rendell, J. C. Burant, S. S. Iyengar, J. Tomasi, M. Cossi, N. Rega, J. M. Millam, M. Klene, J. E. Knox, J. B. Cross, V. Bakken, C. Adamo, J. Jaramillo, R. Gomperts, R. E. Stratmann, O. Yazyev, A. J. Austin, R. Cammi, C. Pomelli, J. W. Ochterski, R. L. Martin, K. Morokuma, V. G. Zakrzewski, G. A. Voth, P. Salvador, J. J. Dannenberg, S. Dapprich, A. D. Daniels, O. Farkas, J. B. Foresman, J. V. Ortiz, J. Cioslowski, and D. J. Fox, Gaussian, Inc., Wallingford CT, 2010.

34. S. Simon, M. Duran and J. J. Dannenberg, *J. Chem. Phys.*, 1996, **105**.

35. Calculations performed without BSSE correction gave ΔE values that are consistently ca. 10 kcal mol^{-1} lower than the BSSE-corrected values, and show the same trend in substituent effects (see Table S1 in ESI).

36. Additional calculations of the association energies of **2F** and **4F** were performed at the M06-2X/6-311++G(d,p)//M06-2X/6-31+G(d,p) level of theory. Y. Zhao and D. G. Truhlar, *Theor. Chem. Acc.*, 2008, **120**, 215-241. In the case of **2F**, the energetics favor the parallel geometry, with the association energy of the parallel *anti* geometry (–7.6 kcal/mol) being slightly lower than that of the antiparallel *anti* geometry (–7.3 kcal/mol). In the case of **4F**, the association energy of the antiparallel geometry (–11.2 kcal/mol) is lower that of the parallel geometry (–9.8 kcal/mol). These results are consistent with those of the MP2/6-311++G(d,p)//MP2/6-31+G(d,p) calculations reported in Table 2.

Table 1. Transition temperatures (°C) and enthalpies of transitions (kJ mol^{-1}, in parentheses) for compounds **QL20-*m/n*-*x*F**, **QL22-8/8-*x,y*F$_2$** and **QL27-8/8** measured by DSC.

Compound	Cr		SmC		SmA	N		I
QL20-8/8-2F	•	66 (56)	•	80[a]	•		83 (9.3)	•
QL20-8/8-3F	•	81 (42)	(•	72)[a,c]	•		96 (12)	•
QL20-8/8-4F	•	82 (46)			•		102 (10)	•
QL20-10/6-2F	•	72 (37)	•	85[a]	•		88 (9.2)	•
QL20-10/6-3F	•	87 (50)	(•	75)[a,c]	•		106 (12)	•
QL20-10/6-4F	•	93 (41)			•		114 (12)	•
QL20-12/4-2F	•	91	(•	85)[a,c]	•		93 (49)[b]	•
QL20-12/4-3F	•	120 (52)			(•		116 (8.5))[c]	•
QL20-12/4-4F	•	120 (51)			•		133 (13)	•
QL22-8/8-2,3F$_2$	•	81 (63)	(•	78)[a,c]	•		88 (11)	•
QL22-8/8-2,4F$_2$	•	62 (56)	(•	61)[a,c]	•		92 (10)	•
QL22-8/8-2,5F$_2$	•	75 (42)	•	76[a]	•		87 (10)	•
QL22-8/8-2,6F$_2$	•	36 (22)	•	68 (2.5)		•	75 (1.7)	•
QL22-8/8-3,4F$_2$	•	78 (51)			•		98 (8.9)	•
QL22-8/8-3,5F$_2$	•	88 (52)			•		95 (12)	•
QL27-8/8	•	36 (19)	•	65[a]	•		92 (9.3)	•

[a] Transition temperature measured by polarized microscopy. [b] Total enthalpy for both transitions due to partial resolution of the peaks. [c] Monotropic mesophase.

Table 2. Potential energies of association ΔE for unsubstituted and fluoro-substituted *n*-butyloxybenzene dimers in parallel and antiparallel geometries.[a]

	ΔE (kcal mol^{-1})[b]			
X	*Parallel-Syn*	*Parallel-Anti*	*Antiparallel-Syn*	*Antiparallel-Anti*
H	–6.8		–6.5	
2F	–6.2	–7.5	–4.3	–6.5
3F	–6.2	–6.8	–6.3	–6.4
4F	–8.1		–9.2	

[a] Based on BSSE-corrected energies obtained at the MP2/6-311++G**//MP2/6-31+G** level of theory. [b] Calculated as the difference between the BSSE-corrected energy of the associated dimer and twice the energy of one molecule obtained at the MP2/6-311++G**//MP2/6-31+G** level.